Surfactant-Assisted Route to Synthesize Well-Aligned ZnO Nanorod Arrays on Sol−Gel-Derived ZnO Thin Films

ARTICLE *in* THE JOURNAL OF PHYSICAL CHEMISTRY B · AUGUST 2006

Impact Factor: 3.3 · DOI: 10.1021/jp062729l · Source: PubMed

5 AUTHORS, INCLUDING:

Dev Apurba
KTH Royal Institute of Technology
34 PUBLICATIONS **651** CITATIONS
SEE PROFILE

Subhendu K Panda
Central Electrochemical Research Institute
40 PUBLICATIONS **801** CITATIONS
SEE PROFILE

Soumitra Kar
Haldia Institute of Technology, Haldia, India
82 PUBLICATIONS **2,587** CITATIONS
SEE PROFILE

Surfactant-Assisted Route to Synthesize Well-Aligned ZnO Nanorod Arrays on Sol−Gel-Derived ZnO Thin Films

Apurba Dev,[†] Subhendu K. Panda,[†] Soumitra Kar,[†] Supriya Chakrabarti,[‡] and Subhadra Chaudhuri*[,†]

Department of Materials Science, Indian Association for the Cultivation of Science, Kolkata-700032, India, and Department of Physics and Electronics, Graduate School of Engineering, Osaka Prefecture University, Japan

Received: May 4, 2006; In Final Form: June 6, 2006

Anisotropic growth of ZnO nanorod arrays on ZnO thin films was achieved at a temperature of 90° C by a surfactant-assisted soft chemical approach with control over size and orientation. ZnO thin films with *c*-axis preferred orientation had been achieved by the sol−gel technique. Lengths, diameters, and the degree of alignment of the ZnO nanorods were controlled by changing the experimental parameters. It was observed that the surfactant was essential to restrict the lateral growth of the nanorods, whereas the pH level of the reaction medium controlled the length of the nanorods. On the other hand, the orientation of the nanorods depended on the crystalline orientation of the film as well as the pH of the reaction medium. Room-temperature photoluminescence studies revealed that the ZnO nanorods with the best alignment exhibited the best emission property. The ZnO nanorods exhibited a strong UV emission peak at ∼3.22 eV, ascribed to the band-edge emission. The field emission studies of the well-aligned nanorod arrays exhibited a low turn-on field of 1.7 V/μm to get an emission current density of 0.1 μA/cm^2.

Introduction

Zinc oxide is a wide band gap (3.37 eV) semiconductor with a large binding energy (60 meV) possessing unique optical and electronic properties. It is a key material of technological importance because of its several fascinating properties that have vast applications in photonic, field emission, and sensing devices. The lack of a center of symmetry in wurtzite crystal and large electrochemical coupling result in strong piezoelectric and pyroelectric properties in ZnO that have important applications such as mechanical actuators and piezoelectric sensors[1]. In addition, ZnO exhibits diverse group growth morphology in the nanoregime that has made this material a promising candidate in the field of nanotechnology. Among the various nanoforms, one-dimensional (1-D) oriented nanostructures, such as nanorods, nanowires, nanotubes, nanopins, and so forth, are particularly important for efficient field emission, which has enormous commercial applications such as field emission flat panel displays,[2] X-ray sources,[3] vacuum microwave amplifiers,[4,5] and so forth. With their high melting point, good thermal and chemical stability, and low electron affinity,[6] ZnO 1-D arrays are a promising alternative to carbon nanotubes for field emitters with long lifetimes. Moreover, the successful demonstration of UV lasing action[7] from ZnO has added a new direction in the field of nanotechnology and motivated subsequent research for the fabrication of 1-D ZnO nanostructured arrays with precise control over size, shape, and orientations. The ability to build oriented assemblies of 1-D nanostructures is also very attractive for the fabrication of future photonic,[8−9] field emission,[10] and sensing[11] devices. As a consequence, several synthetic methodologies have been proposed. Gas-phase growth techniques such as chemical vapor deposition, physical vapor deposition, metalorganic vapor phase epitaxy, vapor liquid solid, and so forth[12−15] have been successfully employed to grow ZnO nanorods and nanowires on solid substrates. However, these methods are very expensive and require high temperature. Recently, a solution phase approach to fabricate aligned ZnO nanorods was utilized.[16−21] This technique has many advantages, as it is cost-effective, and large scale-up production is possible. In addition, oriented seed-initiated synthesis[22] has been found to be very effective to produce highly aligned ZnO nanorod arrays. This technique[22] is suitable to prepare long free-standing ZnO nanorods, which exhibit efficient field emission as long as their aspect ratio is high. But increase in length is generally accompanied by subsequent increase in diameter. So, if a proper approach is adopted to restrict the lateral growth without affecting the orientation of the nanorods, they could be expected to exhibit efficient field emission properties for their high aspect ratio and excellent orientation. In addition, the ability to choose the crystallographic growth direction of a nanorod array aids in tuning the physical properties of the material, including spontaneous piezoelectric polarization, thermal and electrical conductivity, dielectric constant, lattice strain, and so forth.

In this paper, we are reporting a soft chemical approach to fabricate long and vertically aligned ZnO nanorod arrays with crystallographic orientation over sol−gel-derived ZnO thin films. The role of different experimental parameters was explored with a view to achieve diameter-controlled well-aligned ZnO nanorod arrays.

Experimental Section

Preparation of ZnO Film. For the preparation of the ZnO thin film, zinc acetate dihydrate [$Zn(CH_3COO)_2 \cdot 2H_2O$] was added in dry ethanol, and, subsequently, a few drops of diethanolamine (DEA) were added with continuous stirring for

* To whom correspondence should be addressed. Tel: +91-033-2473-4971. Fax: +91-033-2473-2805. E-mail address: mssc2@iacs.res.in.
[†] Indian Association for the Cultivation of Science.
[‡] Osaka Prefecture University.

10.1021/jp062729l CCC: $33.50
Published on Web 07/06/2006

1 h. An optimized amount of basic DEA was added to the solution to enhance the dissolution of the Zn salt. Properly cleaned quartz, silicon, and glass plates were used as the substrates. The substrates were coated with the sol by a dip-coating technique and subsequently dried in an oven at 80 °C for 5 min. This process was repeated six times to increase the film thickness, and final films were annealed in air at 600 °C for 30 min. The entire process was repeated three times further to ensure complete and uniform coverage of ZnO seeds. Finally, transparent ZnO films were obtained, which were utilized as the substrates for the formation of the ZnO nanorod arrays.

Preparation of ZnO Nanorods. For the preparation of ZnO nanorods, 10 mmol of sodium dodecyl sulfate (SDS) and 1 mmol of zinc acetate dihydrate were added to 30 mL of xylene and stirred for 1 h. Then hydrazine hydrate (80%) diluted with ethanol was added to the solution very slowly. After 1 h of stirring, previously prepared transparent ZnO films were immersed in the solution and refluxed at 90 °C for 5 h. Finally, the substrates covered with a white layer were washed in distilled water and dried in room temperature. The films thus obtained were used for further characterization.

Characterization. The crystalline phase of the products was determined by X-ray power diffraction by a Seifert 3000P diffractometer with Cu K_α radiation ($\lambda = 1.54178$ Å). The compositional analysis was done by energy-dispersive analysis of X-rays (EDAX; Kevex, Delta Class I). The morphology of the samples was determined by a scanning electron microscope (Hitachi; S-2300). Microstructure and crystal structures of the products were further studied through a high-resolution transmission electron microscope (HRTEM; JEOL 2010). Optical absorbance was recorded by a spectrophotometer (Hitachi; U-3410). Optical absorbance spectra of the ZnO samples (both thin films and nanorod films) were directly measured by placing the films perpendicular to the direction of the incident light. Contributions of the substrates (glass or quartz) to the absorption spectra of ZnO samples were eliminated by subtracting the corresponding absorption spectrum of the bare substrates. Photoluminescence (PL) measurements were carried out with a luminescence spectrometer (Hitachi; FL 2500). Raman spectra were recorded using a (SPEX 1403) monochromator equipped with a direct current detection device. The 488 nm laser line of an Ar ion laser was used for excitation with an output power of 20 mW.

Results and Discussion

X-ray diffraction (XRD) was performed on the ZnO films both before and after the formation of nanorods. The XRD pattern of the transparent ZnO thin film prior to the nanorod growth is shown in Figure 1a. A strong and sharp diffraction peak corresponding to the (002) crystal plane of ZnO revealed the preferred orientation of the film along the *c*-axis of ZnO crystals. It was observed that the results were independent of the substrates (silicon, quartz, and glass) used. The XRD pattern (Figure 1b) of the nanorod arrays indicates that the nanorods are well aligned and grow along the [0001] direction following the seed's crystal orientation. The composition of the nanorods was determined by an EDAX study (Figure 1c), which revealed the presence of Zn and O as the elementary components in stoichiometric amounts.

The morphologies and dimensions of the nanorods were studied through scanning electron microscopy (SEM) and transmission electron microscopy (TEM) observations. Figure 2a shows the SEM image of a ZnO thin film, revealing the uniform distribution of the ZnO seeds on a quartz substrate.

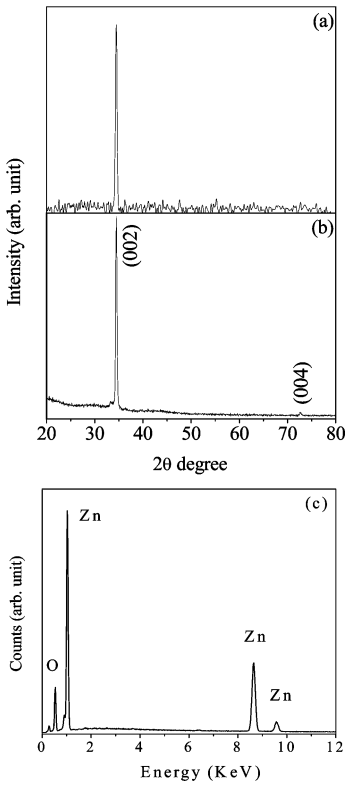

Figure 1. XRD pattern of (a) ZnO film on quartz substrate and (b) ZnO nanorod arrays. (c) EDAX pattern recorded over a representative ZnO nanorod array.

Figure 2b is the low magnification image of the ZnO nanorod arrays, showing uniformity of the nanorods over a large area. The image in the inset of Figure 2b reveals that the cross-section of the nanorods is hexagonal. The image demonstrates that the orientation of the nanorods is quite good, and the nanorods grow normal to the substrate. The nanorods have diameters ranging from 80 to 100 nm with lengths of $\sim 3\ \mu$m. The magnified tilted view of the nanorods (Figure 2c) reveals that the nanorods are well separated from each other.

With a view to investigate the role of the surfactant (SDS) and the base hydrazine hydrate in the dimension and degree of orientation of the ZnO nanorod arrays, we have carried out a series of experiments, and the results are listed in Table 1. ZnO nanorod arrays were also synthesized without using SDS, following an identical experimental procedure. It was observed that, in all the cases, the growth of the nanorods in the lateral dimensions was quite high. The SEM image shown in Figure 3a reveals that the diameters of the resulting nanorods increased to around 500 nm within 2 h of refluxing. Thus, these results indicate that the presence of the surfactant (SDS) was essential to regulate the lateral growth of the ZnO nanorods.

Hydrazine hydrate is a strong base, and it was used to regulate the pH of the solution. The pH level of the reaction medium was also varied within a certain range, keeping the amount of the surfactant and all other experimental parameters unchanged to investigate its effect on the ZnO nanorod arrays. Initially, the pH of the solution was measured to be 6.5 when hydrazine hydrate was not added. An experiment was also carried out under this condition, keeping the other parameters identical, and the SEM studies of the resultant film revealed that ZnO nanorods did not grow on the ZnO-coated substrate. In the next experiment, the pH of the solution was raised to 10.6 by adding the proper amount of hydrazine hydrate in the solution, which was then stirred for 1 h, followed by 5 h refluxing. Under these

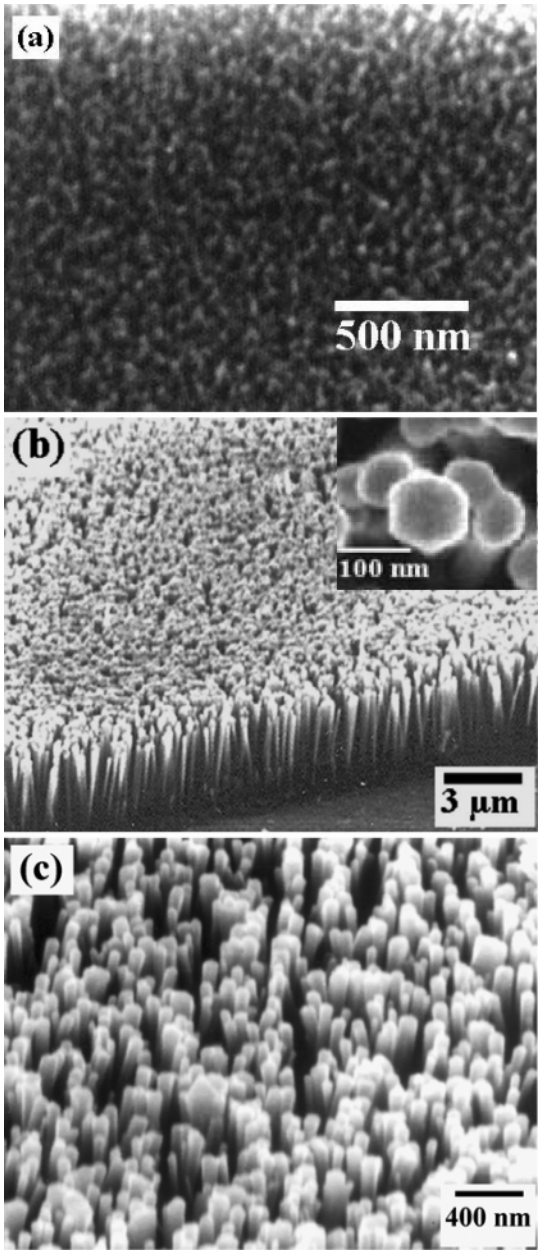

Figure 2. SEM image of (a) ZnO seed and (b) ZnO nanorod arrays over a large surface. The inset shows the hexagonal tip of the nanorods. (c) Tilted view of the nanorod arrays.

TABLE 1: Brief Summary of the Experimental Details and Corresponding Results

sample	pH of the solution	surfactant	reaction time (h)	diameter of the nanorod (nm)	length of the nanorod (μm)
S1	10.6	with SDS	5	~60	2
S2	11.3	with SDS	5	80−100	3
S3	11.6	with SDS	5	~120	6
S4	11.9	with SDS	3	200−250	3
S5	11.9	with SDS	5	200−250	7
S6	11.6	without SDS	2	~500	2

conditions, uniform growth of aligned ZnO nanorods having diameters of ~60 nm and lengths of ~2 μm was observed (Figure 3b). With further increase of the pH of the solution to 11.3, the diameters of the resulting nanorods were found to increase to around 80−100 nm, while the lengths of the nanorods increased to 3 μm (Figure 3c). There was a further increase in length and diameter when the pH of the solution was increased to 11.6. The SEM image of the sample prepared at this condition is shown in Figure 3d, revealing that the diameters of the nanorods were ~120 nm, and the lengths were ~6 μm. It can be observed that the increase in the lengths of the nanorods was much higher compared to that of their diameters with increasing the pH level of the solution. Because of this abrupt increase in the length of the nanorods, the free-standing nature of the nanorods was lost, and instead they coalesced to each other at their tips. The diameter of the nanorods increased further to around 200−250 nm (Figure 3e) within 3 h of refluxing when the pH of the solution was raised to 11.9, but under these conditions, the orientation of the nanorods collapsed, resulting in nonaligned products (Figure 3e). A total collapse of the free-standing nature of the nanorods was noticed when the solution was refluxed for 5 h at this pH level (Figure 3f).

To investigate the effect of the crystallographic orientation of the ZnO thin films on the nanorod arrays, two experiments were carried out using ZnO thin films having no *c*-axis texturing effect. The pH of the solution was maintained at 11.3 and 11.6, respectively. The XRD pattern of ZnO thin film substrate and the as-prepared ZnO nanorod arrays are shown in Figure 4a,b, respectively. It can be observed that, in addition to the diffraction from the (002) crystal planes, two more diffraction peaks corresponding to the (100) and (101) crystal planes of ZnO appeared in the XRD pattern of the ZnO thin film. However, in the nanorod samples, these peaks were quite weak relative to the (002) peak. This could be attributed to the anisotropic growth of the ZnO nanorods along the (002) direction. The SEM images corresponding to pH 11.3 and 11.6 are shown in Figure 5a,b, respectively. It can be observed that, despite possessing quite identical diameters, the orientations of the nanorods prepared on the non-*c*-axis-orientated ZnO thin films (Figure 5) were poor compared to samples S2 and S3 (Figure 3c,d, respectively) prepared with the *c*-axis-oriented films under identical experimental conditions.

TEM was also performed to further investigate the size and crystallinity of the ZnO nanorods. Figure 6a shows the low magnification bright-field TEM image of a single nanorod having a length of ~3 μm. The selected-area electron diffraction (SAED) pattern (inset of Figure 6a) reveals that the nanorod is single crystalline in nature. The lattice spacing estimated from the HRTEM image (Figure 6b) of a single nanorod was found to be around 0.26 nm, which corresponds to the (0002) planar spacing of ZnO in the wurtzite phase. Figure 6c is the TEM image of nanorods formed in a higher concentration of hydrazine hydrate (S3). It can be observed that the nanorods have a length of ~6 μm and a diameter of ~120 nm.

In growing 1-D nanostructures, there are two important steps that control the quality of the products. The first one is the nucleation, which initiates the growth of 1-D nanostructures. In this synthesis process, *c*-axis-oriented ZnO thin films were used. These seeded films served as nucleation sites and also provided crystallographic growth direction to the resulting nanorods. The second step is the growth, and for 1-D structures, it is important to achieve anisotropic growth with good control over size, shape, and orientation. The structure of ZnO wurtzite crystal can be described as a number of alternating planes composed of tetrahedrally coordinated O^{2-} and Zn^{2+} ions stacked along the *c*-axis[1]. These oppositely charged ions produce positively charged Zn(0001) and negatively charged O(000−1) surfaces, resulting in a spontaneous polarization along the *c*-axis. As a result, the ZnO surface attracts opposite charges (Zn^{2+} or OH^-) from the solution, forming $Zn(OH)_2$. In this

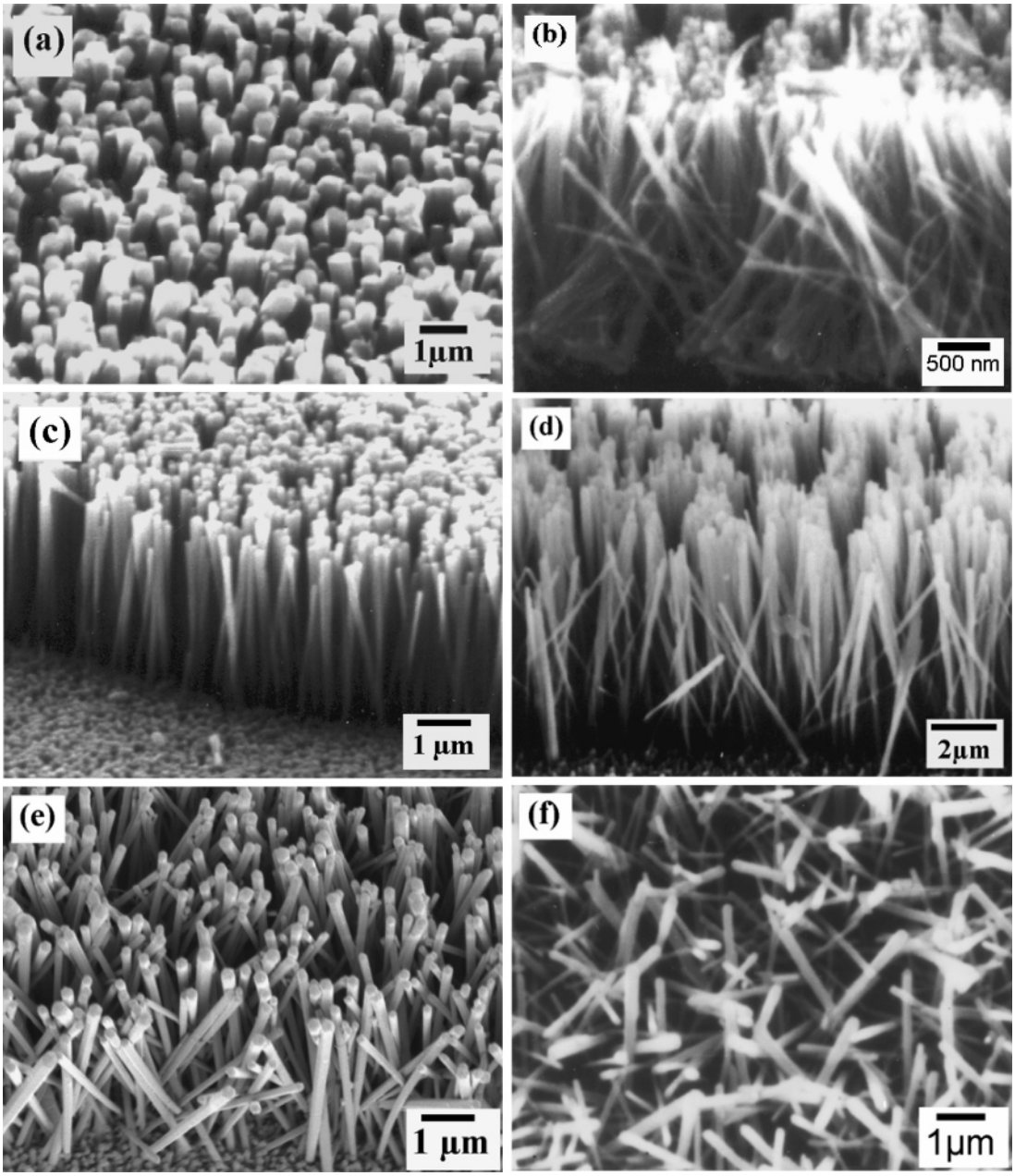

Figure 3. SEM images of nanorods prepared under different experimental conditions as listed in Table 1: (a) S6, (b) S1, (c) S2, (d) S3, (e) S4, and (f) S5.

experiment, SDS plays an important role in controlling the lateral growth of the nanorods. The surfactant molecules at a higher concentration are believed to form rodlike micelles,[21,23−25] which entrap the Zn^{2+} and OH^- ions and form $Zn(OH)_2$. These rodlike micelles are stable at low temperatures[21,24] (<100° C), and, during the period of refluxing, the $Zn(OH)_2$ molecules within the micelles begin to decompose. Also, the elevated temperature may increase the activity of SDS, causing the micelles to collide with each other and thus increasing the length of the nanorods. It can be seen from Figure 3e,f that there was an increase in length only when the period of refluxing was increased from 3 to 5 h. However, in addition to the above-mentioned mechanism, the possibility of other mechanisms being responsible for the restriction of the lateral growth cannot be ruled out. For example, it is also possible that, instead of forming rodlike micelles, the surfactant molecules get absorbed on the side surface of ZnO nanorods,[26] restricting the lateral growth. The question that remains at this stage is, Why should the diameter of the nanorods increase with increasing pH of the solution? The increase in pH of the solution leads to the formation of more $Zn(OH)_2$ and thus an increase in the concentration of $Zn(OH)_2$ in the solution. So, if there is a concentration difference of $Zn(OH)_2$ between the inside and outside of the rodlike micelles, there may be a transfer of $Zn(OH)_2$ from outside to inside the micelles through the surface of the micelles,[23] and thus the diameter of the resulting nanorods would increase. The experiments conducted with (Figure 3c) and without (Figure 3a) SDS certainly confirm that the diameter of the nanorods can be well controlled by using surfactant. The synthesis approach described here is also suitable to vary the length of the nanorods within a wide range by using the proper amount of hydrazine hydrate.

Figure 7a shows the room-temperature optical absorbance spectra of *c*-axis-oriented ZnO thin film and the aligned ZnO nanorod arrays. A sharp absorption edge at 368 nm corresponding to 3.37 eV was observed from both the samples. This

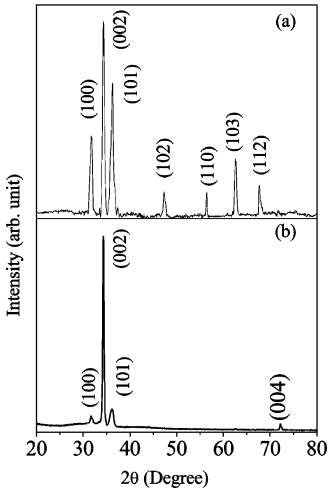

Figure 4. (a) XRD spectra of ZnO film having no crystallographic orientation. (b) ZnO nanorod arrays prepared on the above ZnO film.

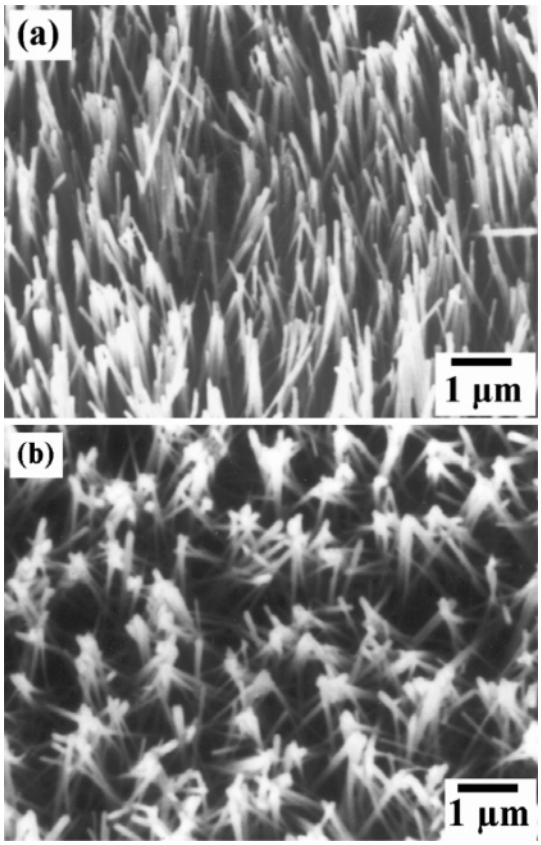

Figure 5. SEM image of the ZnO nanorod arrays prepared on ZnO film having no crystallographic orientation at pH values of (a) 11.3 and (b) 11.6.

corresponds to bulk values of the band gap of ZnO. The absorption study also revealed that the as-prepared ZnO nanorod arrays are transparent in the visible region. The PL property of ZnO was widely investigated for its potential applications in UV photonic devices. This is also an important tool to evaluate crystal defects. The room-temperature PL spectra of the as-prepared ZnO thin film and the nanorod arrays are shown in Figure 7b. The PL spectra of all the samples show very strong emissions at 3.22 eV, which is generally attributed to the excitonic emission.[27] It was also observed that the intensity of the excitonic emission depends on the degree of alignment of the ZnO nanorods. It was observed that the intensity of the UV

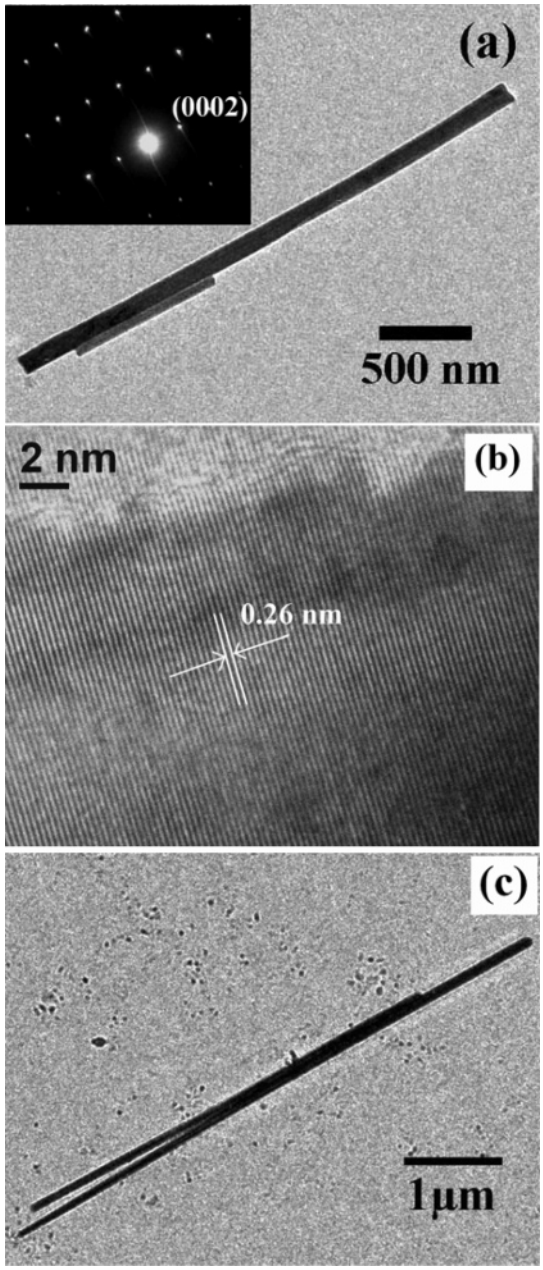

Figure 6. (a) TEM image of a single nanorod, with the inset showing the corresponding SAED pattern. (b) HRTEM image of a nanorod and (c) TEM image of a long nanorod (S3).

emission peak was maximum for sample S2, having the best alignment, and least for the randomly oriented nanorods in sample S5. The intensity of the emission from the ZnO thin films was quite low compared to that of the nanorod arrays, and the PL plot of the ZnO thin film was multiplied by a factor for better visibility. It can be observed that, in addition to the excitonic emission, the PL spectrum of ZnO film consists of a broad emission in the visible green region (Figure 5c). This green light emission peak originated as a result of the transition from defect states.[11,28] However, this defect level emission was very weak in the PL spectrum of ZnO nanorods. So it is clear that the defect concentration could be substantially reduced by this synthesis approach. Figure 7c shows the PL spectra of the ZnO nanorods produced on the ZnO thin film, having no preferred orientation along the *c*-axis, both before and after the formation of nanorods. The results indicated that the defect-related green emission was quite strong in the normal ZnO thin

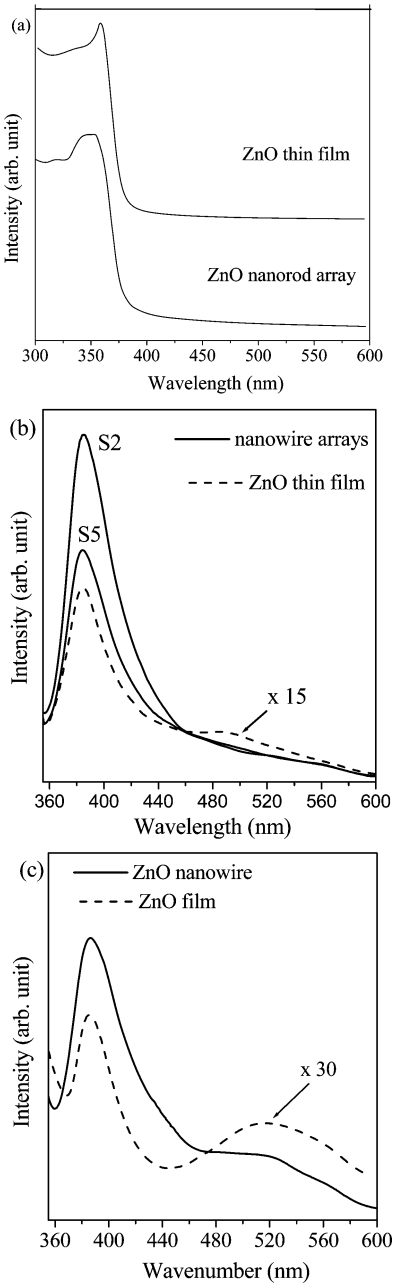

Figure 7. (a) Room-temperature optical absorption spectra of the ZnO thin film with crystallographic orientation. (b) PL spectra of the *c*-axis-orientated ZnO films before and after the formation of ZnO nanorod arrays. (c) PL spectra of the ZnO films having no crystallographic orientation both before and after the formation of ZnO nanorod arrays.

film compared to that of the *c*-axis-orientated ZnO thin film, indicating the presence of a relatively lower defect concentration in the *c*-axis-oriented ZnO thin films. ZnO nanorod arrays produced over this type of ZnO thin film also exhibited a weak green emission band along with the strong UV emission peak. Thus, these results indicate that the optical quality of the ZnO nanorod arrays produced by this synthesis approach improves with the alignment of the nanorods. The PL studies of ZnO nanorod,[29] nanowire,[30] and nanonail[11] arrays produced by the high-temperature-based thermal evaporation approach revealed that these arrays exhibited a strong defect-related emission band along with the excitonic UV emission. Thus, ZnO nanorod arrays having a good UV emission property could be synthesized by this surfactant-assisted approach.

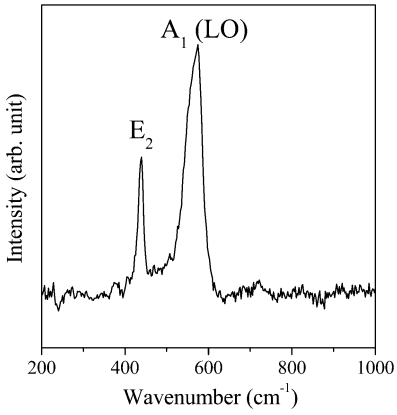

Figure 8. Raman spectra of a representative ZnO nanorod array (S2).

Raman scattering is sensitive to the microstructure of nano-sized materials. We performed the Raman scattering of one representative ZnO nanorod array to investigate the vibrational properties. Figure 8 shows the Raman spectrum of the ZnO nanorod arrays recorded at room temperature. Two strong peaks positioned at 437 and 574 cm^{-1} are observed. Wurtzite ZnO belongs to the C^4_{6v} ($P6_3mc$) space group. The primitive cell includes two formula units, with all atoms occupying the 2b sites of symmetry, C_{3v}. At the Γ point of Brillouin zone, group theory predicts the existence of the following optic modes: $\Gamma_{opt} = A_1 + 2B_1 + E_1 + 2E_2$. The frequency from the B_1^{low} and B_1^{high} silent modes has been calculated at 260 and 540 cm^{-1}, respectively. The A_1, E_1, and E_2 modes are Raman active. In addition, A_1 and E_1 are infrared active, and therefore they split into longitudinal and transverse optical (LO and TO) components. The mode assignment under ambient conditions is well established in the literature.[31,32] The peak at 437 cm^{-1} has been attributed to the E_2^{high} mode, and 574 cm^{-1} peak has been assigned to the A_1 (LO) mode in the low-wavenumber region. The red shift of the Raman peak in the nanomaterials is usually related to the phonon confinement effect, defects, and strains. The appearance of the E_2^{high} and A_1 (LO) mode exactly in the bulk position of the ZnO[31] of our samples implies that the nanorods are of high crystallinity and almost free of defects and strains.

The field emission properties of the ZnO nanorods have been investigated by several other groups, and the reports in the literature indicate that well-aligned and well-separated ZnO nanorod arrays are better field emitters. So we measured the field emission properties of the ZnO nanorod arrays having the best alignment and well-separated nature (S2) by two parallel plate configurations in a vacuum chamber with a pressure of 10^{-7} Torr, and the distance between the electrodes was maintained at 300 μm. The measured current density as a function of electric field is shown in Figure 9a. A very low turn-on electric field of 1.7 V/ μm was obtained at an emission current density of 0.1 $\mu A/cm^2$, which reaches 10 $\mu A/cm^2$ at an electric field of 1.9 V/ μm. This value of turn-on electric field is significantly lower than that of ZnO nanopencils,[33] ZnO nanoneedles,[34] and ZnO nanorods coated with amorphous carbon.[35] According to the Fowler−Nordheim (F−N) model, the electron emission from a semi-infinite flat metallic surface can be expressed in terms of current density (J) and electric field E as

$$J = A(\beta^2 E^2/\varphi) \exp(-B\varphi^{3/2}/\beta E) \quad (1)$$

where A and B are constants ($A = 1.54 \times 10^{-10}$ (A V^{-2} eV), B

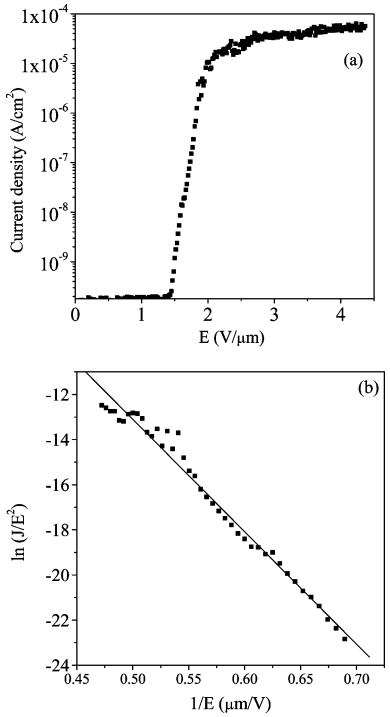

Figure 9. (a) J/E plot of the field emission from the ZnO nanorod array having the best orientation and (b) the corresponding F−N plot.

$= 6.83 \times 10^9$ (V m^{-1} eV$^{-3/2}$)), and φ is the work function. β, the field enhancement factor of the sample is associated with the magnitude of the electric field at the emitting surface by the relation $E(\text{local}) = \beta E$, where E(local) is the local electric field at the emitting top surface. Figure 9b shows the plot of J/E^2 versus $1/E$, exhibiting linear dependencies, which is in agreement with (F−N) eq 1. The value of field enhancement factor β can be estimated from the slope of the F−N plot if the value of work function φ is known. If we assume the work function (φ) is 5.3 eV, the value of β is calculated to be ∼1730, which is much higher than other recent reports on ZnO.[36−37] The field enhancement factor usually depends on the geometry, tip size, length, and number density of the nanorods grown on a substrate.[38] For high aerial densities of nanorods, the local field at the emitting surface reduces as a result of the electrostatic screening effect provoked by the neighboring nanorods. In addition, long and highly oriented nanorods exhibit much better field emission than short and randomly oriented nanorods.[39−40] The vertical growth of the ZnO nanorods has better ability to enhance the local field at the emitting surface and reduce the turn-on electric field.[38] The excellent field emission property of as-prepared ZnO nanorod arrays can be attributed to their good orientation and high aspect ratios.

Conclusion

We have successfully prepared ZnO thin films with a preferred *c*-axis texturing by the sol−gel technique and fabricated well-aligned ZnO nanorod arrays with tunable lengths up to 6 μm on these ZnO films by using a simple surfactant-assisted approach. The diameters of the nanorods were successfully reduced by using surfactant. Well-aligned ZnO nanorod arrays can be prepared over any substrate as long as a uniform *c*-axis-textured uniform ZnO film can be grown on it. High uniformity of the arrays can also be maintained over a large area by this novel approach. The optical properties of as-prepared nanorod arrays show their good crystalline quality. These films of long and aligned ZnO nanorods also exhibited very efficient field-emission properties with a turn-on field as low as 1.7 V/μm and a high field enhancement factor (β). These films of highly oriented nanorod array have potential application in photonics, field emission displays, nanoelectronics, and gas sensing devices.

References and Notes

(1) Wang, Z. L. *Materials Today* **2004**, *7*, 26.
(2) Baughman, R. H.; Zakhidov, A. V.; de Heer, W. A. *Science* **2002**, *297*, 787.
(3) Senda, S.; Sakai, Y.; Mizuta, Y.; Kita, S.; Okuyama, F. *Appl. Phys. Lett.* **2004**, *85*, 5679.
(4) Milne, W. L.; Teo, K. B. K.; Amaratunga, G. A. J.; Legagneux, P.; Gangloff, L.; Schnell, J. P.; Semet, V.; Binh, V. T.; Groening, O. *J. Mater. Chem.* **2004**, *14*, 933.
(5) Saito, Y.; Uemura, S. *Carbon* **2000**, *38*, 169.
(6) Fancher, C. A.; de Clercq, H. L.; Thomas, O. C.; Robinson, D. W.; Bowen, K. H. *J. Chem. Phys.* **1998**, *109*, 8426.
(7) Huang, M. H.; Mao, S.; Feick, H.; Yan, H.; Wu, Y.; Kind, H.; Weber, E.; Russo, R.; Yang, P. *Science* **2001**, *292*, 1897.
(8) Pan, Z. W.; Mahurin, S. M.; Dai, S.; Lowndes, D. H. *Nano Lett.* **2005**, *5*, 723.
(9) Wang, X. D.; Summers, C. J.; Wang, Z. L. *Nano Lett.* **2004**, *4*, 423.
(10) Li, Y.; Lin, P.; Lee, C. Y.; Tseng, T. Y. *J. Appl. Phys.* **2004**, *95*, 3711.
(11) Kar, S.; Pal, B. N.; Chaudhuri, S.; Chakravorty, D. *J. Phys. Chem. B* **2006**, *110*, 4605.
(12) Bae, S. Y.; Seo, H. W.; Park, J. *J. Phys. Chem. B* **2004**, *108*, 5206.
(13) Lyu, S. C.; Zhang, Y.; Lee, C. J.; Ruh, H.; Lee, H. J. *Chem. Mater.* **2003**, *15*, 3294.
(14) Park, W. I.; Kim, D. H.; Jung, S. W.; Yi, G. C. *Appl. Phys. Lett.* **2002**, *80*, 4232.
(15) Gao, P. X.; Wang, Z. L. *J. Phys. Chem. B* **2004**, *108*, 7534.
(16) Greene, L. E.; Law, M.; Goldberger, J.; Kim, F.; Johnson, J. C.; Zhang, Y.; Saykally, R. J.; Yang, P. *Angew. Chem., Int. Ed.* **2003**, *42*, 3031.
(17) Yu, H.; Zhang, Z.; Han, M.; Hao, X.; Zhu, F. *J. Am. Chem. Soc.* **2005**, *127*, 2378.
(18) Dev, A.; Kar, S.; Chakrabarty, S.; Chaudhuri, S. *Nanotechnology* **2006**, *17*, 1533.
(19) Li, Q.; Kumar, V.; Li, Y.; Zhang, H.; Marks, T. J.; Chang, R. P. H. *Chem. Mater.* **2005**, *17*, 1001.
(20) Li, Z.; Ding, Y.; Xiong, Y.; Yang, Q.; Xie, Y. *Chem.—Eur. J.* **2004**, *10*, 5823.
(21) Guo, L.; Ji, Y. L.; Xu, H.; Simon, P.; Wu, Z. *J. Am. Chem. Soc.* **2002**, *124*, 14864.
(22) Greene, L. E.; Law, M.; Tan, D. H.; Montano, M.; Goldberger, J.; Somorjai, G.; Yang, P. *Nano Lett.* **2005**, *5*, 1231.
(23) Xiong, Y.; Xie, Y.; Yang, J.; Zhang, R.; Wu, C.; Du, G. *J. Mater. Chem.* **2002**, *12*, 3712.
(24) Zhang, J.; Zhang, S. Y.; Chen, H. Y. *Chem. Lett.* **2004**, *33*, 1054.
(25) Lv, R.; Cao, C.; Guo, Y.; Zhu, H. *J. Mater. Sci.* **2004**, *39*, 1575.
(26) Sun, X. M.; Chen, X.; Deng, Z. X.; Li, Y. D. *Mater. Chem. Phys.* **2002**, *78*, 99.
(27) Liang, J.; Liu, J.; Xie, Q.; Bai, S.; Yu, W.; Qian, Y. *J. Phys. Chem. B* **2005**, *109*, 9463.
(28) Roy, V. A. L.; Djurisic, A. B.; Chan, V; Gao, J.; Lui, H. F.; Surya, C. *Appl. Phys. Lett.* **2003**, *83*, 141.
(29) Hsu, N. E.; Hung, W. K.; Chen, Y. F. *J. Appl. Phys.* **2004**, *96*, 4671.
(30) Lyu, S. C.; Zhang, Y.; Ruh, H.; Lee, H. J.; Shim, H. W.; Suh, E. K.; Lee, C. J. *Chem. Phys. Lett.* **2002**, *363*, 134.
(31) Calleja, J. M.; Cardona, M. *Phys. Rev. B.* **1977**, *16*, 3753.
(32) Decremps, F.; Porres, J. P.; Saitta, A. M.; Chervin, J. C.; Polian, A. *Phys. Rev. B* **2002**, *65*, 092101.
(33) Wang, R. C.; Liu, C. P.; Huang, J. L.; Chen, S. J.; Tseng, Y. K.; Kung, S. C. *Appl. Phys. Lett.* **2005**, *87*, 013110.
(34) Li, Y. B.; Bando, Y.; Golberg, D. *Appl. Phys. Lett.* **2004**, *84*, 3603.
(35) Liao, L.; Li, J. C.; Wang, D. F.; Liu, C. S.; Fu, Q; Fan, L. X. *Nanotechnology* **2005**, *16*, 985.
(36) Cui, J. B.; Daghlian, C. P.; Gibson, U. J.; Püsche, R.; Geithner, P.; Ley, L. *J. Appl. Phys.* **2005**, *97*, 044315.
(37) Ham, H.; Shen, G.; Cho, J. H.; Lee, T. J.; Seo, S. H.; Lee, C. J. *Chem. Phys. Lett.* **2005**, *404*, 69.
(38) Li, S. Y.; Lin, P.; Lee, C. Y.; Tseng, T. Y. *J. Appl. Phys.* **2004**, *95*, 3711.
(39) Nilsson, L.; Groening, O.; Emmenegger, C.; Kuettel, O.; Schaller, E.; Schlapbach, L.; Kind, H.; Bonard, J.-M.; Kern, K. *Appl. Phys. Lett.* **2000**, *76*, 2071.
(40) Banerjee, D.; Ho, S. J.; Ren, Z. F. *Adv. Mater.* **2004**, *16*, 2028.